Analytica Chimica Acta 821 (2014) 34–40

Contents lists available at ScienceDirect

Analytica Chimica Acta

journal homepage: www.elsevier.com/locate/aca

Electrochemical detection of benzo(a)pyrene and related DNA damage using DNA/hemin/nafion–graphene biosensor

Yongnian Ni [a,b,*], Pingping Wang [b], Haiyan Song [b], Xiaoyun Lin [a,b], Serge Kokot [c]

[a] State Key Laboratory of Food Science and Technology, Nanchang University, Nanchang 330047, China
[b] Department of Chemistry, Nanchang University, Nanchang 330031, China
[c] School of Chemistry, Physics and Mechanical Engineering, Science and Engineering Faculty, Queensland University of Technology, Brisbane 4001, Australia

HIGHLIGHTS

- Construction of a novel DNA/hemin/nafion-graphene/GCE biosensor.
- DNA damage induced by the benzo(a)pyrene metabolite was detected.
- DPV analysis of benzo(a)pyrene provided a quantitative estimate of DNA damage.
- Hemin/H_2O_2 system could mimic the cytochrome P450 to metabolize benzo(a)pyrene.

GRAPHICAL ABSTRACT

A novel electrochemical biosensor, DNA/hemin/nafion–graphene/GCE, was constructed to quantitatively study the DNA damage induced by the metabolite of benzo(a)pyrene in the presence of H2O2.

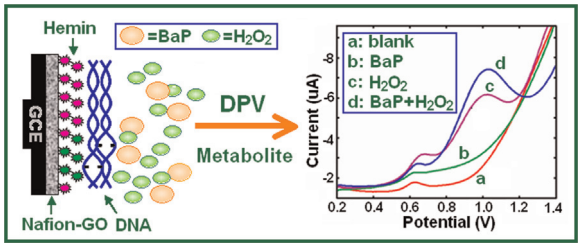

ARTICLE INFO

Article history:
Received 24 January 2014
Received in revised form 5 March 2014
Accepted 7 March 2014
Available online 12 March 2014

Keywords:
DNA damage
Polycyclic aromatic hydrocarbons
DNA/hemin/nafion–graphene/glassy carbon electrode
Differential pulse voltammetry
DNA biosensor

ABSTRACT

A novel electrochemical biosensor, DNA/hemin/nafion–graphene/GCE, was constructed for the analysis of the benzo(a)pyrene PAH, which can produce DNA damage induced by a benzo(a)pyrene (BaP) enzyme-catalytic product. This biosensor was assembled layer-by-layer, and was characterized with the use of cyclic voltammetry, electrochemical impedance spectroscopy (EIS) and atomic force microscopy. Ultimately, it was demonstrated that the hemin/nafion–graphene/GCE was a viable platform for the immobilization of DNA. This DNA biosensor was treated separately in benzo(a)pyrene, hydrogen peroxide (H_2O_2) and in their mixture, respectively, and differential pulse voltammetry (DPV) analysis showed that an oxidation peak was apparent after the electrode was immersed in H_2O_2. Such experiments indicated that in the presence of H_2O_2, hemin could mimic cytochrome P450 to metabolize benzo(a)pyrene, and a voltammogram of its metabolite was recorded. The DNA damage induced by this metabolite was also detected by electrochemical impedance and ultraviolet spectroscopy. Finally, a novel, indirect DPV analytical method for BaP in aqueous solution was developed based on the linear metabolite *versus* BaP concentration plot; this method provided a new, indirect, quantitative estimate of DNA damage.

1. Introduction

Polycyclic aromatic hydrocarbons (PAHs) are compounds, which have fused aromatic rings, and are potent atmospheric pollutants [1]. In general, the main sources of PAHs include automobile exhaust fumes and smoke from combustion of organic material [2,3]. PAHs, especially with four or more ring structures, and their metabolites, are mutagenic and toxic compounds with significant human health risk [4,5]. Benzo(a)pyrene (BaP) is the basic PAH compound with five structural rings, and is classified as a potential carcinogen [6–9]. However, it was found that BaP could not directly cause genetic damage; in fact, it is classified as a procarcinogen, i.e., a compound which becomes carcinogenic only

* Corresponding author at: Department of Chemistry, Nanchang University, Nanchang 330031, China. Tel.: +86 791 83969500; fax: +86 791 83969500.
E-mail addresses: ynni@ncu.edu.cn (Y. Ni), s.kokot@qut.edu.au (S. Kokot).

http://dx.doi.org/10.1016/j.aca.2014.03.006
0003-2670/

after it undergoes changes by metabolic processes [10]. Generally, *in vivo*, BaP is catalyzed by the cytochromes such as P450 (CYP), to form the BaP-7,8-dio-9,10-epoxide (BPDE), which is the major carcinogen causing DNA damage [11,12]. In addition, BaP covalently bonds to DNA, mainly with the base, guanine, to form BDPE-DNA adducts [13–15], and two oxidation DPV peaks corresponding to guanine and adenine residues inside the double helix of DNA are at about +0.75 V and +1.05 V, respectively, with a bare GCE in pH 4.5 acetate buffer [16].

Cytochrome P450 is a powerful catalyst, which can catalyze many types of reaction such as epoxidation and hydroxylation [17] as well as hydroxylation of the C—H bonds, even in the presence of a C=C bond [18]. Recently, it was found that horseradish peroxidase and hydrogen peroxide, (HRP)/H_2O_2, could mimic cytochrome P450 in metabolic processes, especially during epoxidation [19,20]. This approach was used to develop a new model to mimic and directly detect the DNA damage induced by acrylamide and its metabolites [21]; the $(DNA/HRP)_n$/graphene-ionic liquid-nafion modified electrode was immersed in an acrylamide and H_2O_2 solution to metabolize the acrylamide into glycidamide; the DNA damage was then detected by the acrylamide and its metabolite. Most natural enzymes are expensive and can be readily inactivated by a variety of physical and chemical factors; thus, their usage in the catalyst industry has been restricted. More recently, metal porphyrins were synthesized to mimic hydrogen peroxidase in order to overcome the strict reaction conditions and the high costs [22–24]. Other researchers developed enzymes to mimic the cytochrome P450, glutathione peroxidase (GPX), and chloroperoxidase (CPO), and these novel enzymes have been stabilized on biosensors, which were then used for analysis [25–27]. Also, it was found that a simple metal porphyrin, hemin ($C_{34}H_{32}ClFeN_4O_4$, CAS number: 16009-13-5), could mimic HRP [28].

For a potential biosensor, it is particularly important to have hemin and DNA immobilized on the electrode's surface. Thus, it was observed [29] that hemin could intercalate into DNA because it is a large molecule with planar porphyrin; also, it was found [30] that hemin interacted with covalently immobilized calf-thymus DNA. Consequently, DNA biosensors were constructed to include hemin, and this electrochemical probe was used to investigate damaged DNA. Such work indicated that it is possible to construct stable DNA/hemin modified electrodes. In addition, it is known that graphene has properties, which include fast electron transportation, large specific surface area and good biocompatibility; hence, it was used for the construction of different types of sensor [31–33], in which graphene's π–π bonds could interact with the porphyrin of the hemin [34]. Vanlentini et al. [35] have applied a carbon nano-material film to immobilize hemin for amperometric H_2O_2 and NO_2^- detection. Consequently, such work provided a theoretical basis for the application and development of hemin/graphene modified electrode.

BaP may be analysed by many different techniques, e.g., high performance liquid chromatography with mass spectrometry (HPLC-MS) [36], ultra performance liquid chromatography with mass spectrometry (UPLC-MS) [37], synchronous fluorescence spectroscopy [38], kinetic spectrometric three dimensional chemiluminescence [39], and amperometric biosensor [40]. However, most are time consuming, moderately expensive and complex. Development of electrochemical methodology for the analysis of BaP offers an alternative approach, which could overcome some of the above shortcoming.

The aims of this research work were: (1) to investigate if the hemin/H_2O_2 system could be a substitute for the cytochrome P450 in the case of a PAH/DNA interaction; (2) to research and develop a novel DNA/hemin/nafion–graphene/GCE biosensor for the detection of BaP-mediated DNA damage and test its potential as an analytical tool for indirect, quantitative analysis of BaP in aqueous solution.

2. Materials, instrumentation and methods

2.1. Materials and reagents

All experiments were performed with analytical grade reagents, and doubly distilled water was used throughout. A stock solution of BaP (5.0×10^{-4} mol L^{-1}, Sigma–Aldrich Co., Shanghai) was prepared by dissolving a suitable amount of its crystals in acetone; this solution was diluted further with the same solvent to obtain another solution (1.0×10^{-5} mol L^{-1}). Hemin solution (2.0 mg mL^{-1}, Sigma–Aldrich Co., Shanghai) was prepared by dissolving 50 mg hemin in 25 mL 5.0×10^{-3} mol L^{-1} sodium hydroxide solution. The calf-thymus DNA (type 1, D1501; Sigma Chemical Co. Shanghai) was used as received. A DNA solution (1.0 mg mL^{-1}) was prepared by dissolving 50.0 mg DNA in 50 mL 25.0 mmol L^{-1} sodium chloride solution. A fresh solution of 0.39 mol L^{-1} H_2O_2 was prepared daily. All solutions used in the experiments were adjusted with the 0.1 mol L^{-1} phosphate buffer (PBS, pH 7.4), which was prepared by mixing suitable amounts of 0.1 mol L^{-1} KH_2PO_4 with Na_2HPO_4. Graphene was obtained from Chengdu Organic Chemicals Co., Chinese Academy of Sciences, and nafion was purchased from Sigma–Aldrich Co., Shanghai, China.

2.2. Instrumentation

All the electrochemical measurements were performed on a CHI 660 A electrochemical workstation (Chenhua, Shanghai, China). The working glassy carbon electrode (GCE), a platinum auxiliary and an Ag/AgCl reference electrode formed a conventional three-electrode system, which was used for electrochemical measurements. UV–vis absorbtion spectra were recorded with an Agilent 8453 spectrophotometer (Aglient Technologies, Santa Clara, CA, USA) equipped with a 1.0 cm quartz cell. The Atomic force microscope (AFM) images were measured with the use of an AJ-III instrument (Shanghai Aijian Nanotecnology, China) in the tapping mode. Standard silicon cantilevers were used at their typical resonance frequencies 60–150 kHZ. Orion SA720 meter (USA) was used to monitor the buffer pH, and mica sheets were purchased from the General Research Institute Shanghai, China.

2.3. Layer-by-layer electrode assembly

First, a GCE was polished, in order, with alumina slurries of different particle size (1.0, 0.3, and 0.05 μm), and then, this polished electrode was sonicated sequentially in dilute nitric acid (0.5 M), ethanol and deionized water, each for 5 min. This GCE was then activated by repeated potential scanning between −1.0 and 1.0 V in 10 mL 0.25 mol L^{-1} sulfuric acid until a reproducible cyclic voltammogram was obtained. For the electrode modification process, 1.0 mg graphene was dispersed in 1.0 mL 0.5% nafion solution, which was then ultrasonicated for 2 h to form a homogenous mixture of graphene–nafion. This mixture (20 μL) was deposited dropwise onto the activated GCE surface and dried in air for 4 h. Subsequently, 10 μL 2.0 mg mL^{-1} hemin and 10 μL 1.0 mg mL^{-1} DNA were added, in succession, onto the nafion–graphene modified electrode, and it was allowed to dry, in air, for 12 h. The obtained biosensor was then immersed in the PBS buffer (pH 7.4), and gently shaken for about 5 min so as to remove any loosely adsorbed hemin and DNA.

Before the AFM experiment, mica sheets were cleaved with an adhesive tape, and then nafion–graphene, hemin/nafion–graphene and DNA/hemin/nafion–graphene systems were immobilized on such sheets according to the above procedure described for the GCE.

2.4. Instrumental procedures

2.4.1. Electrochemical detection of the DNA damage

To detect the BAP metabolite and verify the mimicing effect of the hemin/H_2O_2 system, the DNA/hemin/nafion–graphene/GCE biosensor was immersed in 2.0×10^{-7} mol L^{-1} BaP solution (200 μL 1.0×10^{-5} mol L^{-1} BaP solution mixed with 10 mL blank solution (2 mL pH 7.4 PBS and 8 mL distilled water)); 2.0×10^{-3} mol L^{-1} H_2O_2 (50 μL 0.39 mol L^{-1} H_2O_2 transferred to 10 mL blank solution), and the mixed solution (2.0×10^{-7} mol L^{-1} BaP + 2.0 $\times 10^{-3}$ mol L^{-1} H_2O_2) for 10 min, respectively. Finally, each modified electrode surface was thoroughly washed with double distilled water, and the pretreated biosensor was submitted to DPV analysis over the potential range of +0.2 to +1.4 V with a scan rate of 100 mV s^{-1} in 10 mL blank pH 7.4 PBS solution, respectively. It should be noted that, in this experiment, before each DPV scan, the biosensor was reassembled to insure experimental consistency.

2.4.2. DNA damage detection by EIS and UV–vis spectrophotometry

An electrochemical impedance spectroscopy (EIS) analysis was performed to investigate any DNA damage; the DNA/hemin/nafion–graphene/GCE was immersed into the mixed solution of 2×10^{-7} mol L^{-1} BaP and 2×10^{-3} mol L^{-1} H_2O_2 for 10 min, and then the EIS mesurements were carried out in 5 mmol L^{-1} [Fe$(CN)_6]^{3-/4-}$ solution for this pretreated biosensor. The frequency range was 0.1–1×10^5 Hz.

UV–vis spectrophotometry was performed to verify any DNA damage induced by the BaP metabolite. The absorption spectra were recorded in the range of 200–900 nm. Since it is known that the absorption of the damaged DNA is stronger than that of the normal dsDNA under the same conditions [21], the absorption of DNA (at about 260 nm) was used as an indicator of DNA damage. However, it has been reported that hemin and BaP have absorptions at 265 and 254 nm, respectively [34,41], and consequently, there may be peak overlaps at the DNA wavelengths. Since, it has been noted that the BaP absorption at the experimental concentration was almost eight or nine times higher than that of DNA and hemin, the UV–vis spectra were corrected for the BaP absorption by subtraction as required. In this work, eight types of analyte solution were investigated in order to extract the information on DNA damage: DNA, DNA + H_2O_2, DNA + hemin, DNA + BaP, DNA + H_2O_2 + BaP, DNA + hemin + BaP, DNA + H_2O_2 + hemin, and DNA + H_2O_2 + hemin + BaP.

2.4.3. Indirect quantitative analysis of BaP

This quantitative analysis relied on the characteristic DPV response of BaP metabolite, i.e., guanine, which was used as an indirect, quantitative indicator of BaP. The DNA/hemin/nafion–graphene/GCE was immersed in BaP solutions with different concentrations (0–220×10^{-9} mol L^{-1} with an interval of 40×10^{-9} mol L^{-1}); these solutions were dissolved in 2×10^{-3} mol L^{-1} H_2O_2 in PBS buffer. Then, each of the DPV measurements was sequentially carried out in a blank solution (pH 7.40 PBS), and the respective voltammograms were recorded in the potential range of +0.2 to +1.4 V at a scan rate of 100 mV s^{-1}. It should be noted that each DPV measurement of pretreated biosensor was performed in 10 mL blank solution (2 mL PBS and 8 mL distilled water), as described in Section 2.4.1.

3. Results and discussion

3.1. Electrochemical characterization of the prepared biosensor

Nafion–graphene, hemin/nafion–graphene and DNA/hemin/nafion–graphene modified GCE electrodes were prepared (Section 2.3), and each one was characterized with the use of CV and the relevant sensor being immersed in 5×10^{-3} mol L^{-1} [Fe$(CN)_6]^{3-/4-}$ solution (Fig. 1A). It was quite evident that a pair of well defined redox peaks were obtained at the untreated GCE with the reduction peak at 0.17 V and the oxidation peak at 0.25 V (Fig. 1A, curve a). However, after the modification of the untreated GCE with nafion–graphene, the redox peak current of this electrochemical probe clearly decreased (Fig. 1A, curve b); this could be attributed to the nafion cation exchange film itself, which resists the diffusion of [Fe$(CN)_6]^{3-/4-}$ anions [42]. When the hemin was deposited on the nafion–graphene modified GCE, it produced a marginally improved profile than that of the nafion–graphene GCE (Fig. 1A, curve c); this observation may be explained by the likely coordination effect between the iron of the hemin and the cyanide group of [Fe$(CN)_6]^{3-/4-}$. Finally, since electrostatic repulsion is likely to occur between DNA and [Fe$(CN)_6]^{3-/4-}$, the CV analysis of the electrochemical probe was more difficult to detect by the DNA/hemin/nafion–graphene modified electrode than the two other biosensors (Fig. 1A, curve d).

Further characterization of the modified electrode was performed with the EIS technique with the use of the same electrodes immersed in the 5×10^{-3} mol L^{-1} [Fe$(CN)_6]^{3-/4-}$ solution. The EIS Nyquist plots (Fig. 1B) of the untreated GCE (curve a), nafion–graphene/GCE (curve b), hemin/nafion–graphene/GCE (curve c) and DNA/hemin/naifon–graphene/GCE (curve d) indicated significant differences between the four types of electrode. Elsewhere, it has been demonstrated that the measured curvature of the EIS profiles is indicative of the charge transfer resistance of the sample [43] – hence, the approximately straight line fit of the EIS responses from the untreated GCE indicated a low electron transfer resistance. When the electron transfer resistance was moderate or high, then it was reflected in the change of curvature of the EIS profile, i.e., changes in the semi-circular diameters. Such

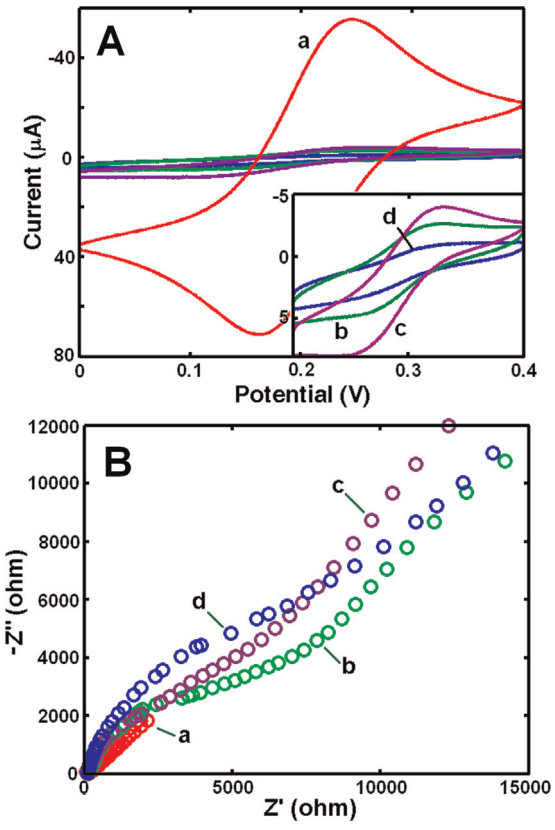

Fig. 1. CVs (A) and EIS (B) of (a) GCE, (b) nafion–graphene/GCE, (c) hemin/nafion–graphene/GCE, and (d) DNA/hemin/nafion–graphene/GCE in 5×10^{-3} mol L^{-1} Fe$(CN)_6^{3-/4-}$ (1:1) solution containing 0.1 mol L^{-1} KCl. Scan rate: 100 mV s^{-1}.

changes were evident to a lesser or greater extent in the high frequency region of the EIS profiles in this work – DNA/hemin/nafion–graphene/GCE showed the strongest semi-circular diameter changes, which were followed by the diminishing effects of the nafion–graphene/GCE and hemin/nafion–graphene/GCE in that order. This indicated that the charge on the $[Fe(CN)_6]^{3-/4-}$ probe was the most difficult to transfer from the solution to the surface of the DNA/hemin/nafion–graphene/GCE; the difficulty decreased in order from the hemin/nafion–garaphene/GCE followed by the nafion–graphene/GCE, respectively. These results were consistent with the conclusions from the CV analysis.

3.2. Surface morphology of various modified electrodes

The AFM images of the nafion–graphene, hemin/nafion–graphene, and DNA/hemmin/nafion–graphene modified electrodes (Fig. 2), indicated that the nafion–graphen flim (Fig. 2A) appeared as if it was constructed from fibrous structures similar to flattened fibres; on the other hand, the image of the hemin/nafion–graphene film displayed a very different, rather finely disordered, granular structure distributed more or less over the fibrous network (Fig. 2B). These findings are consistent with previous work [44]. On the introduction of DNA, the granular units seemed to combine more tightly into more ordered clumps of various sizes but the overall structure appeared to be less ordered and more porous (Fig. 2C). In general, these images reflect the structural changes that occur as the electrode surface is modified layer-by-layer for 10 min, before the introduction of hemin and DNA, respectively.

3.3. Influence of immersion time on DNA damage

In order to investigate the influence of immersion time on the anodic peak current of guanine, the modified DNA/hemin/nafion–graphene electrode was separately immersed in BaP, H_2O_2, and their mixed solutions (solution preparation: see Section 2.4.2), respectively, for the different time periods. From Fig. 3, it can be seen that no obvious anodic peak could be observed, and there was no

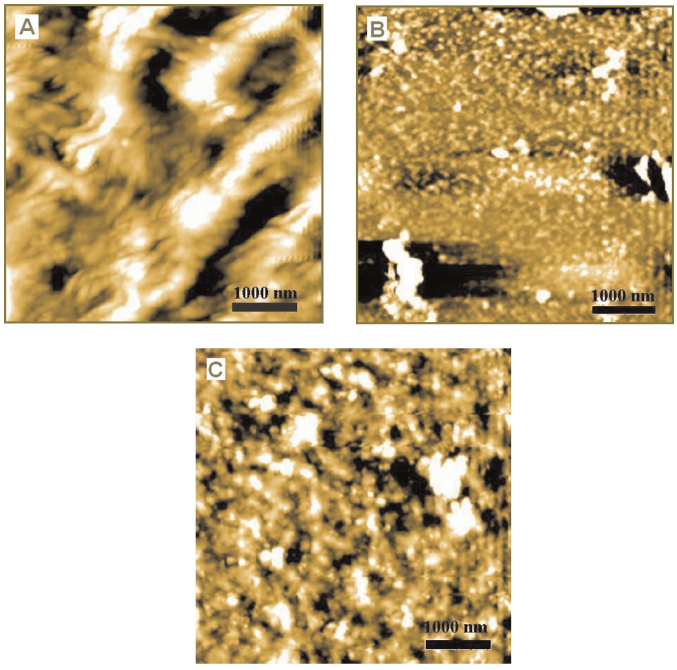

Fig. 2. AFM images of deposits on mica sheet surfaces: (A) nafion–graphene, (B) hemin/nafion–graphene, and (C) DNA/hemin/nafion–graphene.

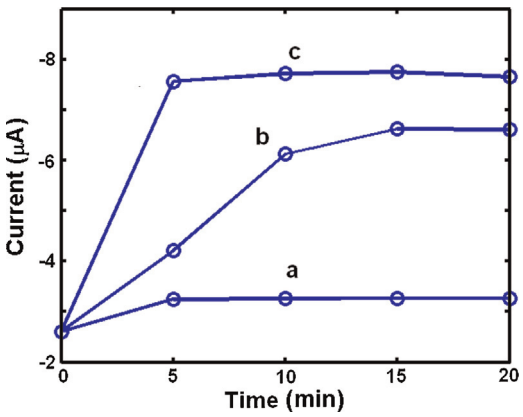

Fig. 3. Relationship between the DPV anodic peak intensity and the immersion time for guanine by using differently pretreated DNA/hemin/nafion–graphene/GCE biosensor in PBS buffer (pH 7.40): (a) untreated, (b) immersed in 2.0×10^{-7} mol L^{-1} BaP solution, (c) 2.0×10^{-3} mol L^{-1} H_2O_2 solution, and (d) 2.0×10^{-7} mol L^{-1} BaP and 2.0×10^{-3} mol L^{-1} H_2O_2 mixed solution.

significant change for the anodic peak of BaP with increasing, immersed time (curve a). In the presence of H_2O_2, it substantially increased with time up to 10 min (curve b), and with the mixed solution (curve c) the current rose rapidly and the curve leveled off between 5 and 10 min. Thus, 10 min was selected as a suitable time for the experiments in further work with this electrode system.

3.4. DPV electrochemical detection of the DNA damage

To investigate DNA damage, which was caused by the BaP-metabolite, the DNA/hemin/nafion–graphene/GCE was immersed separately in three different solutions: 2.0×10^{-7} mol L^{-1} BaP, 2.0×10^{-3} mol L^{-1} H_2O_2, and 2.0×10^{-7} mol L^{-1} BaP + 2.0×10^{-3} mol L^{-1} H_2O_2 for 10 min each; thereafter, the DPV analysis was performed on these treated electrodes immersed in the blank solution (Section 2.4.1).

First, to eliminate any interference from the blank, the untreated modified electrode was analysed in a blank solution (2 mL PBS and 8 mL distilled water), and a small anodic peak was recorded at 0.62 V (Fig. 4A, curve a). A similar peak was observed at the same potential when the nafion–graphene modified electrode (in the absence of DNA and hemin) was measured in the blank solution (Fig. 4A, insert). This indicated that there was an anodic peak for graphene at 0.62 V rather than the anodic peak for DNA. A further experiment with the DNA/hemin/nafion–graphene/GCE, which was treated in a BaP solution, produced a similar result, i.e., a peak at 0.62 V was observed (Fig. 4A, curve b). More importantly, no other oxidation signal was obtained. These observations indicated that BaP could not be metabolized in the absence of H_2O_2. A new anodic peak at 1.0 V was noted after the modified electrode was immersed in the H_2O_2 solution for 10 min (Fig. 4A, curve c); this was consistent with H_2O_2 interacting with hemin to produce the hydroxyl free radicals ($OH^{\bullet}$), and DNA will have been damaged most likely at the guanine site. Then, under the same experimental conditions, the modified electrode was immersed into a BaP and H_2O_2 solution at the same concentration, and as expected, a significant increase in the intensity of the anodic peak was observed (Fig. 4A, curve d). This indicated that BaP could be oxidized by hemin in the presence of H_2O_2 to produce a new carcinogenic substance (BaP-metebolite), which could cause significant DNA damage. Consequently, this work has indicated that BaP is a typical procarcinogen, and strongly suggested that the hemin/H_2O_2 system could mimic cytochromes such as the P450. Thus, a new *in vitro* model to mimic and detect DNA damage has been successfully demonstrated.

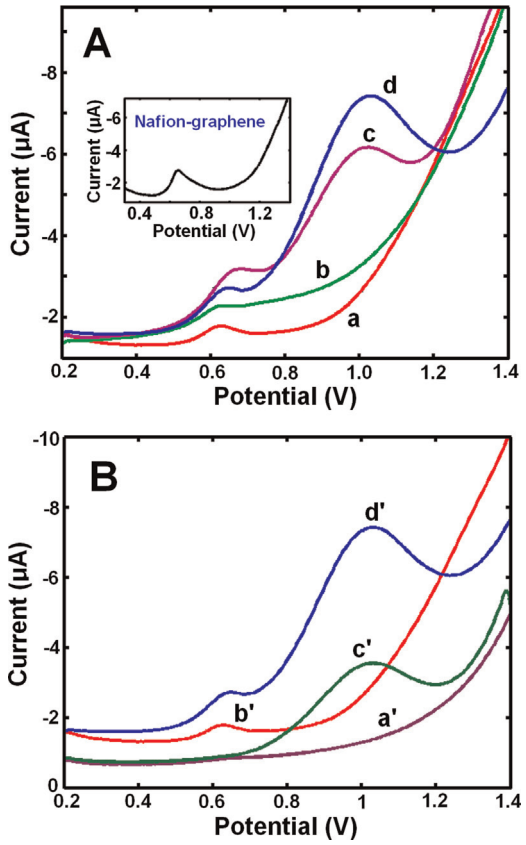

Fig. 4. (A) DPV voltammograms obtained by the DNA/hemin/nafion–graphene/GCE in PBS buffer (pH 7.40): (a) untreated, (b) immersed in 2.0×10^{-7} mol L^{-1} BaP solution, (c) 2.0×10^{-3} mol L^{-1} H_2O_2 solution, and (d) 2.0×10^{-7} mol L^{-1} BaP and 2.0×10^{-3} mol L^{-1} H_2O_2 mixed solution. Insert: DPV of nafion–graphene/GCE in PBS buffer (pH 7.40); (B) DPV voltammograms obtained with the DNA/hemin/GCE (curves a′ and c′) and DNA/hemin /nafion–graphene/GCE (curves b′ and d′) in PBS buffer (pH 7.40). (a′) and (b′): untreated, and (c′) and (d′): immersed in 2.0×10^{-7} mol L^{-1} BaP and 2.0×10^{-3} mol L^{-1} H_2O_2 mixed solution for pretreatment.

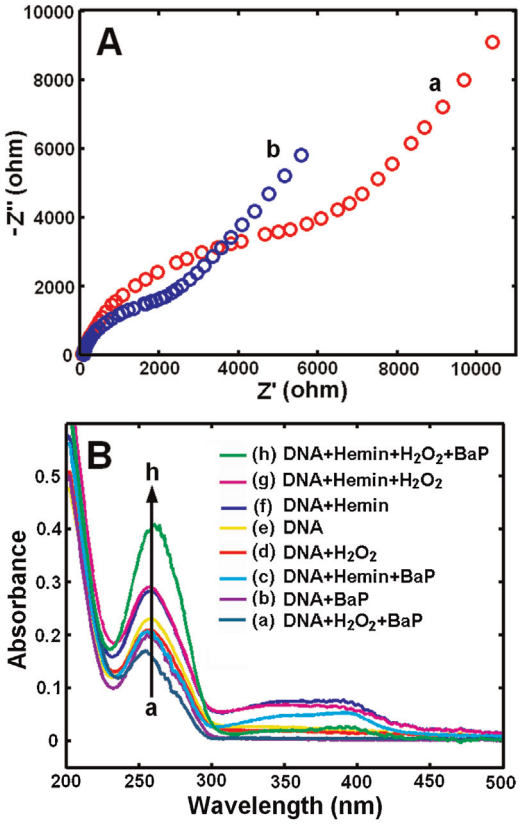

Fig. 5. (A) EIS recorded in the 5.0×10^{-3} mol L^{-1} $[Fe(CN)_6]^{3-/4-}$ solution with the use of: (a) DNA/hemin/nafion–graphene, (b) immersion in 2.0×10^{-7} mol L^{-1}BaP and 2.0×10^{-3} mol L^{-1} H_2O_2 mixed solution for 10 min. (B) UV–vis spectra of 12 μg mL^{-1} DNA in: (a) 5.0×10^{-4} mol L^{-1} $H_2O_2 + 8.0 \times 10^{-8}$ mol L^{-1} BaP, (b) 8.0×10^{-8} mol L^{-1} BaP, (c) 0.8 μg mL^{-1} hemin + 8.0×10^{-8} mol L^{-1} BaP, (d) 5.0×10^{-4} mol L^{-1} H_2O_2, (e) blank, (f) 0.8 μg mL^{-1} hemin, (g) 0.8 μg mL^{-1} hemin + 5.0×10^{-4} mol L^{-1} H_2O_2, (h) 0.8 μg mL^{-1} hemin + 5.0×10^{-4} mol L^{-1} $H_2O_2 + 8.0 \times 10^{-8}$ mol L^{-1} BaP.

The influence of the electrode material on DNA damage was further investigated, and DPV analysis was performed in the blank solution before and after the DNA/hemin/GCE and DNA/hemin/nafion–graphene/GCE were treated in BaP and H_2O_2 solution for 10 min. It can be seen that when the DNA/hemin/GCE (Fig 4B, curve a′) and DNA/hemin/nafion–graphene/GCE (Fig 4B, curve b′) were untreated, no apparent anodic peak was present at 1.0 V; this indicated that there was no electrochemical activity at 1.0 V when only DNA itself was present. However, when the treated, modified electrodes were similarly scanned, as expected, a relatively stronger anodic peak was obtained at 1.0 V at the DNA/hemin/nafion–graphene/GCE (Fig 4B, curve d′) than at the DNA/hemin/GCE (Fig. 4B, curve c′). These results showed that graphene was an effective sensing platform for small biomolecules and could improve the sensitivity for DNA damage analysis.

3.5. Detection of DNA damage by the EIS technique and UV–vis spectrophotometry

The EIS technique is well-known for the detection of DNA damage [45], and in this work, it was used to verify such damage induced by a metabolite of BaP; it was demonstrated that the DNA/hemin/nafion–graphene modified electrode displayed high charge transfer resistance, which was caused by the electrostatic repulsion between DNA and $[Fe(CN)_6]^{3-/4-}$ anion in an electrolyte solution (Fig. 5A, curve a). However, when the modified electrode was immersed into the BaP and H_2O_2 solution for 10 min, a decrease in the charge transfer resistance was detected at the DNA/hemin/nafion–graphene/GCE (Fig. 5A, curve b); this possibly occurred because the exposed DNA bases reduced the electrostatic repulsion of the negatively charged redox mediator, ($[Fe(CN)_6]^{3-/4}$) [46].

UV–vis spectrophotometry was also carried out to investigate DNA damage attributed to the benzo(a)pyrene enzyme; also, the technique was applied to investigate the feasibility of the hemin/H_2O_2 system mimicking the benzo(a)pyrene effect enzymatic effects (Fig. 5B). In order to eliminate the interference from BaP, the UV spectrum of this compound was subtracted from the overall spectrum of the reaction system under study (Section 2.4). Thus, DNA has a strong absorption at 260 nm (Fig. 5B, curve e), and after the addition of BaP or H_2O_2 (curves b and d), the UV absorption of DNA was almost the same for the three profiles, a, b and d. However, there was an increase in peak intensity when hemin was added to the DNA solution, and a new UV absorption peak at 400 nm was observed (curve f); in this context, previous research has noted that hemin itself has two absorption peaks at 265 and 400 nm [34]. Hence, the observed increasing absorption at 260 nm and that at 400 nm peak could be attributed to the overlap of the DNA and hemin profiles. The important conclusion from these observations was that neither the BaP and H_2O_2 nor hemin alone could damage DNA. When BaP and H_2O_2 were mixed with DNA (curve a), the absorption of DNA was the same as that with the BaP alone; also, when hemin and H_2O_2 were mixed with DNA, the same UV spectrum was obtained as that with the addition of hemin

alone (curve g). However, when the absorption profile of hemin + BaP + DNA was compared with that of the hemin + DNA, it was found that the intensities of the former decreased markedly at both 260 and 400 nm (curve c). These observations suggested that there was an interaction between hemin and BaP. However, the lower spectral intensities noted above, were less than the spectral absorptions of the DNA; this indicated that the product of the hemin + BaP + DNA interaction in the absence of H_2O_2, could not damage the DNA. Thus, the outcome of this conclusion was that hemin itself could not mimic the effect of cytochrome P450. When all these four substances, i.e. DNA + hemin + Bap + H_2O_2, were mixed together, a significant increase in the intensity of the UV–vis absorption peak at 260 nm was observed, while that of the peak at 400 nm was barely detected (curve h). Thus, collectively, these results indicated that hemin has the same effect on DNA as the cytochrome P450 in the presence of H_2O_2; DNA was damaged by a metabolite of BaP, which was produced by the hemin/H_2O_2 system.

3.6. Reproducibility and stability

The DNA/hemin/nafion–graphene/GCE was prepared five separate times using the same GCE. Each one of these electrodes was immersed into 2.0×10^{-7} mol L^{-1} BaP + 2.0×10^{-3} mol L^{-1} H_2O_2 solution for 10 min and DPV analysis was performed using a blank solution (pH 7.40); the results were compared using the anodic peak attributed to guanine, and the average relative standard deviation (%RSD) was 8.21. This indicated that the reproducibility of this modified electrode was satisfactory. Additionally, the stability of the modified electrode was also estimated, and the sensor was stored in PBS buffer (pH 7.40) for 7 days at about 4 °C and then it used to test DNA damage; the anodic peak attributed to guanine decreased slightly, and the corresponding %RSD value was 9.08. Thus, this result indicated that DNA/hemin/nafion–graphene/GCE has acceptable stability.

3.7. Indirect quantitative analysis of BaP

From the experimental work in Sections 3.1–3.5 above, it was found that BaP could damage DNA via an enzymatic catalytic reaction. As described in Section 2.4.5, the DNA/hemin/nafion–graphene/GCE was immersed for 10 min into each of several BaP solutions; each solution had a different concentration – 0, 2.0, 6.0, 10.0, 14.0, 18.0, and 22.0×10^{-8} mol L^{-1}, each in 2×10^{-3} mol L^{-1} H_2O_2 PBS buffer, and the pretreated biosensor was submitted to DPV measurements in the blank solution (pH 7.40 PBS). It was observed that the anodic peak current of guanine

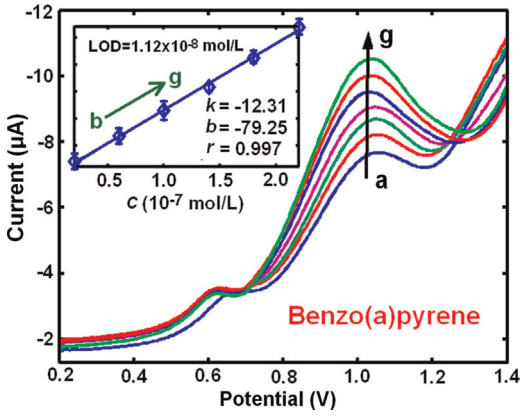

Fig. 6. DPV voltammograms of guanine obtained at the DNA/hemin/nafion–graphene/GCE at different concentrations of BaP (a–g): 0, 2.0, 6.0, 10.0, . . . , 22.0×10^{-8} mol L^{-1}.

Table 1
Results of other published methods for the determination of BaP in comparison with the novel method from this work.

Electrode	Linear range (mol L^{-1})	Limit of detection (mol L^{-1})	Refs.
Amperometric biosensor	$3.31–16.56 \times 10^{-6}$	58.57 (μA mM^{-1})	[40]
Boron-doped diamond electrode	$1.60–20.00 \times 10^{-8}$	2.86×10^{-9}	[47]
Pencil graphite electrode	$2.5–12.5 \times 10^{-7}$	2.7×10^{-8}	[48]
Mercury electrode		1.6×10^{-9}	[49]
DNA/hemin/nafion–graphene/GCE	$2.0–22.00 \times 10^{-8}$	1.12×10^{-8}	This method

increased linearly with the concentration of BaP in the range of 2.0 – 22.0×10^{-8} mol L^{-1} (Fig. 6). The regression equation was:

$$I_p\left(10^{-7}\ \mathrm{A}\right) = -12.3c_{\mathrm{BaP}}\left(10^{-7}\ \mathrm{mol\,L^{-1}}\right) - 79.2 \quad (R = 0.997)$$

The detection limit of BaP was estimated to be 1.12×10^{-8} mol L^{-1}. For comparative purposes, Table 1 lists the linear ranges and detection limits of some other published methods for the determination of BaP against the proposed method [40,47–49]. It can be seen that as compared with these published methods, the sensitivity of this method is similar. Importantly, it is quite evident that it is difficult to detect the content of BaP in aqueous media by classical electrochemical methods; thus, the novel method for BaP analysis, described in this work, is particularly useful in this context.

4. Conclusions

A novel electrochemical biosensor, DNA/hemin/nafion–graphene/GCE, was constructed with the use of the layer-by-layer method on the GCE. It was demonstrated with the use of DPV that this novel biosensor could detect the DNA damage in a solution of BaP + H_2O_2, and the hemin/H_2O_2 system can replace the cytochrome P450. Thus, a chemical processes in this system actually provide an *in vitro* model to mimic the DNA damage *in vivo*. The EIS and UV–vis methods were used to detect the DNA damage induced by the BaP metabolite and to test the feasibility of the hemin/H_2O_2 system in this context, which was designed to mimic the effects of the cytochrome P450. It was demonstrated that this model system could successfully metabolize the BaP PAH molecule to its ultimate carcinogenic form, which facilitated the explanation of the mechanism of the DNA damage induced by BaP.

Subsequently, a novel, indirect DPV method of analysis of BaP in aqueous solution was developed based on the linear changes of anodic current of guanine as a function of the BaP concentration. The results of such analyses indirectly provided a quantitative estimate of DNA damage. This method had a concentration range of 2.0–22.0×10^{-9} mol L^{-1}, with a detection limit of 1.12×10^{-8} mol L^{-1}.

Acknowledgements

The authors gratefully acknowledge the financial support of this study by the National Natural Science Foundation of China (NSFC-21065007), the Education Department Science Foundation of Jiangxi Province (GJJ10037), and the State Key Laboratory of Food Science and Technology of Nanchang University (SKLF-ZZA-201302 and SKLF-ZZB-201303).

References

[1] Y. Sapozhnikova, S.J. Lehotay, Multi-class, multi-residue analysis of pesticides, Analytica Chimica Acta 758 (2013) 80–92.
[2] Y. Segawa, D.W. Stephan, Chemical Communications 48 (2012) 11963–11965.

[3] S. Masala, C. Bergvall, R. Westerholm, The Science of the Total Environment 432 (2012) 97–102.
[4] Z.H. Xia, X.L. Duan, S. Tao, W.X. Qiu, D. Liu, Y.L. Wang, S.Y. Wei, B. Wang, Q.J. Jiang, B. Lu, Y.X. Song, X.X. Hu, Environmental Pollution 173 (2013) 150–156.
[5] L.H. Zhang, P.J. Li, Z.Q. Gong, A.A. Oni, Journal of Enironmental Sciences 18 (2006) 1226–1232.
[6] Internation Agents for Research on Cancer (IARC), Agents Classified by the IARC Monographs, vol. 1–102, Word Health Organization, Lyon, 2011.
[7] P.W. Wester, J.J.A. Muller, W. Slob, G.R. Mohn, P.M. Dortant, E.D. Kroese, Food and Chemical Toxicology 50 (2012) 927–935.
[8] J.R. Liang, H.Y. Zhu, C.Z. Li, Y.C. Ding, Z.J. Zhou, Q. Wu, Toxicology 302 (2012) 285–291.
[9] K.P. Vijayaraman, S. Muruganantham, M. Subramanian, K.P. Shunmugiah, P.D. Kasi, Ecotoxicology and Environmental Safety 86 (2012) 79–85.
[10] J. Padros, E. Pelletier, Marine Environmental Research 50 (2000) 347–351.
[11] M.L. Gao, Y.F. Li, J.G. Long, W. Shah, L. Fu, B.C. Lai, Y.L. Wang, Mutation Research – Genetic Toxicology and Environmental Mutagenesis 719 (2011) 52–59.
[12] S. Ohnishi, S. Kawanishi, Biochemical and Biophysical Research Communications 290 (2002) 778–782.
[13] M.N. Routledge, K.I.E. Mcluckie, G.D.D. Jones, P.B. Farmer, E.A. Martin, Carcinogenesis 22 (2001) 1231–1238.
[14] M. Del Carlo, M. Di Marcello, M. Giuliani, M. Sergi, A. Pepe, D. Compagnone, Biosensors and Bioelectronics 31 (2012) 270–276.
[15] K. Kerman, B. Meric, D. Ozkan, P. Kara, A. Erdem, M. Ozsoz, Analytica Chimica Acta 450 (2001) 45–52.
[16] A.M. Oliveira-Brett, M. Vivan, I.R. Fernandes, J.A.P. Piedade, Talanta 56 (2002) 959–970.
[17] A.D.N. Vaz, D.F. McGinnity, M.J. Coon, Proceedings of the National Academy of Sciences USA 95 (1998) 3555–3560.
[18] S.P. de Visser, The Journal of Physical Chemistry B 111 (2007) 12299–12302.
[19] S. Tafazoli, P.J. O'Brien, Drug Discovery Today 10 (2005) 617–625.
[20] S.P. de Visser, S. Shaik, P.K. Sharma, D. Kumar, W. Thiel, Journal of the American Chemical Society 125 (2003) 15779–15788.
[21] Y.Y.X.J. Qiu. Qu, J. Dong, S.Y. Ai, R.X. Han, Journal of Hazardous Materials 190 (2011) 480–485.
[22] T.G. Traylor, Pure and Applied Chemistry 63 (1991) 265–274.
[23] T.G. Traylor, F. Xu, Journal of the American Chemical Society 109 (1987) 6201–6202.
[24] D. Ostovic, T.C. Bruice, Accounts of Chemical Research 25 (1992) 314–320.
[25] S.P. de Visser, The Journal of Physical Chemistry B 111 (2007) 12299–12302.
[26] G.S. Heverly-Coulson, R.J. Boyd, Journal of Chemical Theory and Computation 8 (2012) 5052–5057.
[27] G. Diaz-Diaz, M.C. Bianco-Lopez, M.J. Lobo-Castanon, A.J. Miranda-Ordieres, P. Tunon-Blanco, Journal of Molecular Catalysis A 353–354 (2012) 117–121.
[28] Y.Z. Li, A. Townshend, Analytica Chimica Acta 340 (1997) 159–168.
[29] F. Qu, Z.W. Zhu, N.Q. Li, Electroanalysis 12 (2000) 831–835.
[30] P. Kara, D. Ozkan, K. Kerman, B. Meric, A. Erdem, M. Ozsoz, Analytical and Bioanalytical Chemistry 373 (2002) 710–716.
[31] T.Y. Chen, P.T.K. Loan, C.L. Hsu, Y.H. Lee, J.T.W. Wang, K.H. Wei, C.T. Lin, L.J. Li, Biosensors and Bioelectronics 41 (2013) 103–109.
[32] D.M. Zhou, Q. Xi, M.F. Liang, C.H. Chen, L.J. Tang, J.H. Jiang, Biosensors and Bioelectronics 41 (2013) 359–365.
[33] A.L. Liu, G.X. Zhong, J.Y. Chen, S.H. Weng, H.N. Huang, W. Chen, L.Q. Lin, Y. Lei, F. H. Fu, Z.L. Sun, X.H. Lin, J.H. Lin, S.Y. Yang, Analytica Chimica Acta 767 (2013) 50–58.
[34] Y.J. Guo, L. Deng, J. Li, S.J. Guo, E.K. Wang, S.J. Dong, ACS Nano 5 (2011) 1282–1290.
[35] F. Valentini, L. Cristofanelli, M. Carbone, G. Palleschi, Electrochimica Acta 63 (2012) 37–46.
[36] A. Bednarikova, B. Sklarsova, E. Kolek, M. Polovka, P. Simko, Polycyclic Aromatic Compounds 31 (2011) 350–369.
[37] S. Zhu, L. Li, C. Thornton, P. Carvalho, B.A. Avery, K.L. Willett, Journal of Chromatography B 863 (2008) 141–149.
[38] T.L. Sposito, M.C. Bisinoti, A.B. Moreira, Analytical Letters 42 (2009) 2271–2279.
[39] J.A.M. Pulgarin, L.F.G. Bermejo, M.N.S. Garcia, I.S.F. Robles, Analytica Chimica Acta 691 (2011) 76–82.
[40] Y.H. Wu, X.Q. Liu, L. Zhang, C.T. Wang, Biosensors and Bioelectronics 26 (2011) 2177–2182.
[41] L.H. Zhang, P.J. Li, Z.Q. Gong, A.A. Oni, Journal of Environmental Sciences 18 (2006) 1226–1232.
[42] X.Y. Lin, Y.N. Ni, S. Kokot, Journal of Hazardous Materials 243 (2012) 232–241.
[43] Z.L. Wang, Y. Kong, C. Yao, Y. Wang, X.F. Ding, Y.S. Zhou, Applied Clay Science 55 (2012) 173–176.
[44] P.H. Yang, Z.J. Zhou, J.Y. Cai, Colloids and Surfaces A 257–258 (2005) 467–472.
[45] M. Gebala, L. Stoica, S. Neugebauer, W. Schuhmann, Electroanalysis 21 (2009) 325–331.
[46] G. Ziyatdinova, J. Labuda, Analytical Methods 3 (2011) 2777–2782.
[47] Y. Yardim, A. Levent, E. Keskin, Z. Senturk, Talanta 85 (2011) 441–448.
[48] E. Keskin, Y. Yardim, Z. Senturk, Electroanalysis 22 (2010) 1191–1199.
[49] A. Nelson, N. Auffret, J. Readman, Analytica Chimica Acta 207 (1988) 47–57.